# Modeling arctic snow distribution and melt at the 1 km grid scale*

**Ming-ko Woo[1] and Kathy L. Young[2]**

[1]McMaster University, Hamilton, Ontario, Canada L8S 4K1. E-mail: *woo@mcmaster.ca*
[2]York University, Toronto, Ontario, Canada M3J 1P3. E-mail: *klyoung@yorku.ca*

Received 1 November 2003; accepted in revised form 18 May 2004

**Abstract** Snow accumulation, re-distribution and melt are important hydrological considerations in the Arctic. This study presents a model of the late-winter snow cover and the ensuing snowmelt in a High Arctic environment at a scale of 1 km. Indexing is used to spread the snow data from a lowland weather station to various terrain units over a $16 \times 13\,km^2$ target area east of Resolute, Cornwallis Island, Canada. Meteorological variables measured at this base station are spatially extended by field derived empirical relationships for the computation of melt at various terrain units using the energy balance approach. These melt rates are weighted by the fractional coverage of various terrain unit within each $1 \times 1\,km^2$ cell. The snow distribution pattern is obtained daily and model performance was tested by comparing observed and computed dates of melt and the radiation balance over snow. The simulated snow pattern compared favourably with the snow cover imaged by LANDSAT. Daily changes in the probability distribution of snow water equivalent over the target area was examined and snow depletion curves were derived. They describe sub-grid variability over an area and our results point to several assumptions that should be scrutinized in sub-grid parameterization of snow distribution.
**Keywords** Depletion curve; energy balance; High Arctic; snow cover; snow modelling; sub-grid parameterization

Nordic Hydrology **Vol 35 No 4–5 pp 295–307** © IWA Publishing 2004

## Introduction

Snow accumulation, re-distribution and melt are normally the dominant hydrological considerations in the Arctic. In the Arctic Islands, the snow cover is highly variable (Woo 1998) and nine to ten months of snow accumulation is often melted within several weeks to generate seasonal high flows. The changing snow distribution pattern strongly affects runoff generation in the melt season. Modelling of snow accumulation, redistribution and ablation processes for small areas in an open environment has been carried out (Essery *et al.* 1999; Liston and Sturm 1998) and subgrid scale snow variation has been generalized by statistical distributions of within-cell snow water equivalent (Liston 2004). The former requires knowledge of snow distribution that may not be transferable between areas; the latter approach, suitable for small areas, demands detailed topographic data and is computationally intense. For application in land surface schemes and macro-scale hydrological models (Frei and Robinson 1998; Pomeroy *et al.* 1998), modelling of sub-grid variations in snow cover and snowmelt is simplified but the simulated outcomes are rarely subject to verification. Satellite surveillance enables the patchiness of the Arctic snow cover to be discerned at the pixel scale but there is no reliable algorithm for the conversion of sensor signals to snow water equivalent or snow depth (Woo *et al.* 1995). With the drainage area of many High Arctic basins lying within the $10^1$ to $10^3\,km^2$ range, but with a drastic decline in hydrometric and climatic stations in the Arctic (Shiklomanov *et al.* 2002), there is a demand to upscale the locally-acquired information and to model snowmelt on grid scales of $10^0$ to $10^1\,km^2$.

*Paper presented at the 14th Northern Research Basins Symposium/Workshop (Kangerlussuaq, Söndre Strömfjord, Greenland, 25–29 August 2003).

In the Canadian Arctic, weather stations and field research sites are mostly confined to the accessible lowland areas. An extension of point data from these locations to estimate the areal snow distribution during the melt season is a necessary step in modelling the changing snow cover and snowmelt runoff from within drainage basins. This study presents a physically based model of snow distribution and melt for the High Arctic environment at a grid scale of 1 km, using snow and meteorological data obtained at a lowland "base" station. The primary focus is on the heterogeneity in snow distribution which strongly affects snowmelt during the brief but intense Arctic melt season. The winter accumulation and redistribution of snow is not considered because operationally it is easier to conduct a late winter snow survey to initialize the snow distribution than to contend with the uncertainties of over-winter snowfall measurement (Goodison 1978) and of estimating sublimation losses (cf. Pomeroy and Essery 1999; Déry and Yau 2001) that may occur throughout the long winter period.

## Study area and field measurements

Data requirements for the model include: (1) terrain unit delineation based on maps and aerial photographs, (2) an end-of-winter snow survey over the target area to obtain initial snow distribution and (3) meteorological data from a single station during the melt period. An area in southwestern Cornwallis Island, Nunavut, was chosen for this study (Figure 1), covering $16 \times 13\,km^2$ to the east of the Resolute Airport (74°45′N, 94°50′W). It is largely devoid of vegetation and terrain plays the dominant role in influencing the snow redistribution due to drifting. Eleven terrain types are recognized, including plateau, dissected plateau, rolling area, lake, valley and slopes of various orientations. Several terrain types occur repeatedly and each is identified as a separate terrain unit so that, in total, the area is divided into 40 units (half of which are valleys at various elevations and of different orientations) based on aerial photographic interpretation and verified in the field (Figure 1). The mean elevation, slope direction and gradient for each unit is also obtained from topographic maps and the areal coverage of various terrain units within the $1 \times 1\,km^2$ grid cells is measured.

At the end of each winter between 1998 and 2002, a snow survey of the target area was conducted using the method described in Yang and Woo (1999). This method involves surveying along transect lines across various identified terrain types. A typical transect is a straight line across the terrain with snow depths taken at regular intervals and with density measured using a Meteorological Service of Canada snow sampler (about one density sample for every 10 depth measurements). The mean snow depth and density permit the calculation of mean snow accumulation on various types of terrain. Field data from each terrain type are used to derive the snow distribution over the target area and the snow cover thus obtained indicates the snow water equivalent (SWE) available for melt in the spring.

To examine variations of several major meteorological variables in different topographical settings and to derive empirical functions for extending point values over different terrain, six automatic weather station sites were set up in 1998 and 1999 about 5 km from the government weather station at Resolute Airport: a main site on flat terrain and five auxiliary sites (in a valley close to the McMaster River, with a gradient of 0.15; on an east-facing slope with a gradient of 0.12; on a southwest-facing slope with a gradient of 0.14; on a northwest-facing slope with a late-laying snowbank and a gradient of 0.14; and on the plateau above the northwest-facing slope site). The flat-land site represents the base station against which the meteorological data of other sites are compared. From 1998 to 2002, it measured incoming and outgoing short-wave radiation, net radiation, air temperature, relative humidity, rainfall, wind speed and wind direction at 1 m height above the snow surface. All data were recorded by a Campbell Scientific CR10 datalogger. The five auxiliary stations measured outgoing short-wave radiation, air temperature, rainfall, relative humidity and wind speed. Air pressure was provided by the government weather station.

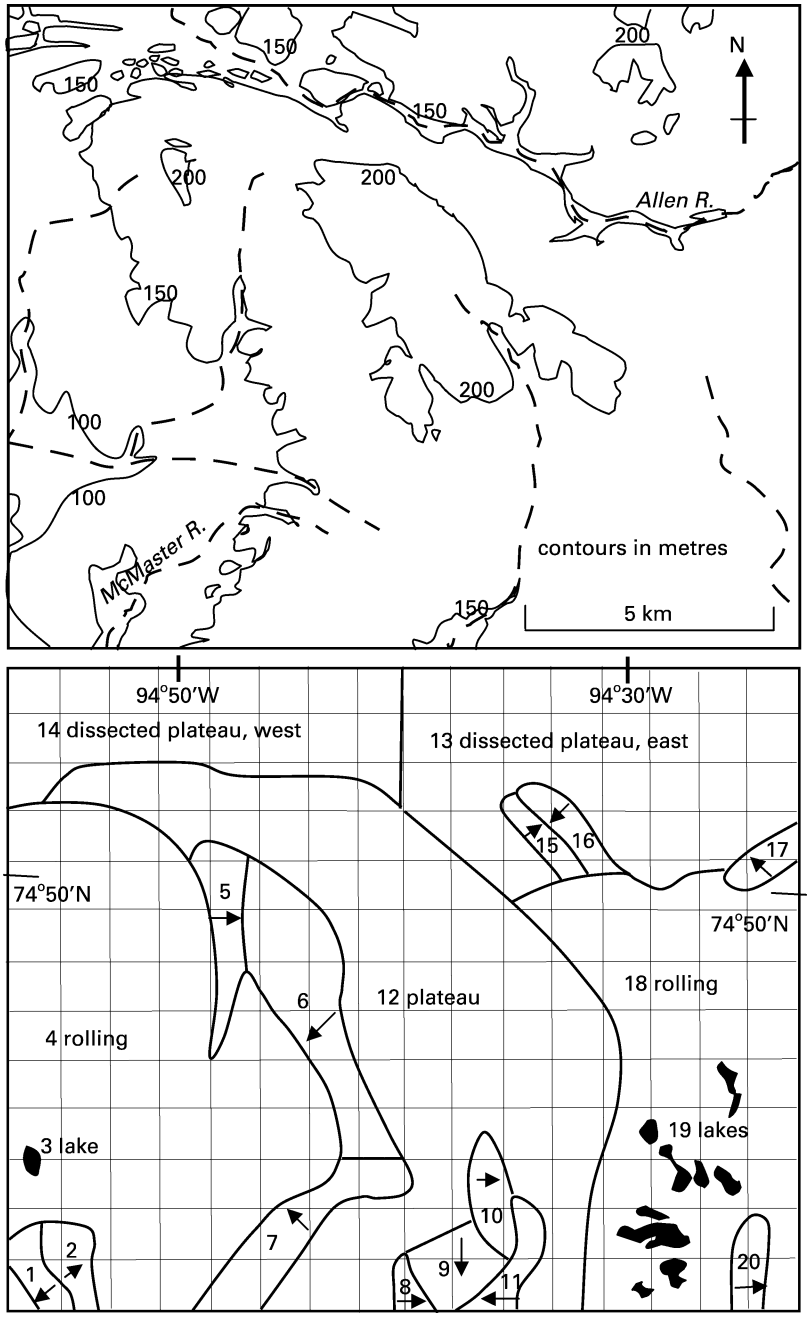


**Figure 1** (top) Topography of the target area in southwestern Cornwallis Island, Nunavut; (bottom) subdivision of the area into terrain units (valleys in various parts of the study area, designated as units 21 to 40, are not shown)

## Computational methods

This study comprises several components which, together, enable the modelling of snow distribution and melt on a 1 km grid scale. The initial end-of-winter snow distribution is first established by an extension of the base station snow measurement over various terrain units in the target area. Then, the driving variables that cause melt are extended to different terrain,

notably the radiation field which is a principal melt energy source. For each terrain unit, snowmelt is calculated using an energy balance approach. The computed results allow accounting of the snow condition for all grid cells to produce daily reports of their residual SWE and fractional snow coverage.



#### Extension of snow cover data

The amount of winter snow accumulation as obtained by the snow surveys showed much inter-annual variation. For instance, there was more snow in the valleys in the spring of 1997 than for the subsequent two years. However, the general pattern of snow distribution for all years confirms the control by the terrain and verifies earlier (Woo 1998) findings that the snow cover pattern does not change from year to year, though the SWE differs annually. Most of the snow drifts into sheltered areas such as gullies and valleys but the snow is generally shallow on exposed terrain, including rolling upland, plateau and lakes. Snow on slopes is variable and changes with local gradient and orientation. Deeper snow tends to be more variable in depth, as larger standard deviations are associated with greater depths.

The snow survey values are compared with the total winter snowfall recorded at the official weather station in Resolute to obtain the SWE indices which are the ratios of the weather station winter snowfall ($P$) and the SWE in various terrain units. These ratios ($r$) are subsequently used to estimate the initial snow storage ($s'$) at each unit $i$

$$s'_i = r_i P \tag{1}$$

#### Comparison of meteorological data among sites

Data collected in 1998 and 1999 at the flat site and at the auxiliary meteorological sites are divided into those for the pre-melt, melt and post-melt periods. Whenever possible, the data collected at the various stations are pooled to examine the intra-cell differences in various meteorological elements. Data from other field studies in the Resolute area are used to obtain additional empirical relationships. The snow temperature at various elevations can be estimated using the values presented in Woo and Ohmura (1997) in which the snow temperature at a particular terrain unit is obtained by

$$T_s(\text{unit}) = T_s(\text{base}) - 10^{(-1.057+0.0095\Delta h)} \tag{2}$$

where $\Delta h$ is the elevation of the terrain unit minus the elevation of the base station (in m). The initial snowpack temperature allows an estimation of the cold content in the snow at the commencement of melt computation.

Hourly temperature differences between the base station and other terrain of similar elevation are obtained by forcing a unit slope to the linear regression relationship. For extension to various terrain, the air temperature of the base station is increased by an empirically obtained value: 0.06°C for plateau, 0.08 and 0.05°C for valley and southwest slopes, and $-0.39$ and $-0.11$°C for east and northeast slopes. To adjust for the elevation effect, an air temperature lapse rate of 0.01°C/m is obtained by comparing the base station temperature with that of a meteorological site set up in the interior of Cornwallis Island, 110 m higher than the flat site (Woo *et al.* 1999). Snow surface temperature ($T_0$) is estimated using air temperature ($T$) of the present ($t$) and the past ($t - 1$) hour (Woo *et al.* 1999):

$$T_s(t) = [T(t-1) + T(t)]/2, \quad \text{if } T(t) < 0 \text{ or } T_s(t) < 0 \tag{3}$$

$$= 0, \quad \text{otherwise.}$$

Relative humidity measured at various meteorological sites are compared using linear regression. The statistics show that the intercepts are significantly different from zero and the

slopes are significantly different from 1.0. However, within the normal range experienced during the snowmelt period (relative humidity between 50 and 100%), the equations yield differences of 5% or less between the base and the other stations. This percentage difference is within the instrumental error. Hence the relative humidity measured at the base station is considered to be applicable to other terrain units without adjustment. For atmospheric pressure, data from the government weather station at Resolute are used. The change of pressure with elevation is calculated using an equation given by Brutsaert (1975):

$$\psi_i = \psi_0 \ \exp\ (-gh_i/RT_b) \tag{4}$$

where $\psi$ is air pressure, $T$ is air temperature, $h$ is elevation and the subscripts $i$ and $b$ refer to the terrain unit and at sea level; $g$ is the acceleration due to gravity and $R$ is the gas constant.

Wind speed at the base station is related to those at other meteorological sites using linear regression. The intercepts are significantly different from zero for the east, southwest and northwest slopes, and the regression slopes are significantly different from 1.0 only for the plateau, valley and northwest slope sites. The intercepts are ignored because of their small magnitude. Then, the ratio of wind speed ratios between a flat site and the plateau, valley and northwest slope are, respectively, 1.09, 0.96 and 0.85.

Incoming short-wave radiation measured at the base station is assumed to be transferable over all locations in the target area. This assumption is unlikely to be valid but the lack of additional measurements and cloud observations at various terrain units makes this approach unavoidable. For sloping terrain, incoming short-wave radiation is adjusted according to the zenith angle and mean terrain gradient, using the algorithm given by Swift (1976).

The albedo decay follows the empirical function established by Woo and Dubreuil (1985):

$$\alpha(\tau) = \alpha_0 - \{(\alpha_0 - \alpha_b)/[\exp(B_1 + B_2\tau)]\} \tag{5}$$

where $\alpha(\tau)$ is the average daily albedo on day $\tau$ after the initiation of melt, $\alpha_0$ is the albedo on the first day of melt and $\alpha_b$ is the albedo of the bare ground. The values of $\alpha_0 = 0.8$ and $\alpha_b = 0.2$ often describe the initial and final albedos of the snow site. Data from the flat site yield $B_1 = 2.46$ and $B_2 = -0.26$ but, for the valley where the snow lingers long, there is a much more gradual decline of the albedo and $B_2$ is found to be $-0.07$. Whenever new snow falls, the albedo rises back to $\alpha_0$ but, after this fresh snow is melted, the exposed old snow surface albedo will be that before the snowfall and the day counter $\tau$ will resume to continue the albedo decline.

#### Snowmelt calculation

Snowmelt is calculated using an energy balance approach, partitioning the melt energy ($Q_m$) into radiation melt, turbulent flux ($Q_t$) that consists of the sensible ($Q_h$) and latent heat ($Q_e$) components, and rain-on-snow melt ($Q_r$):

$$Q_m = Q^* + Q_t + Q_r = (1 - \alpha)\ \mathrm{K}\downarrow + (L\downarrow - L\uparrow) + Q_h + Q_e + Q_r \tag{6}$$

Radiation melt, attributed to the net radiation ($Q^*$), is partitioned into two components: the short-wave component calculated using snow albedo ($\alpha$) and incoming short-wave radiation ($K\downarrow$); and the long-wave calculated as the balance between in-coming ($L\downarrow$) and out-going ($L\uparrow$) components. The albedo is calculated by Equation (5), according to how long the snow at the terrain unit has been melting ($\tau$). Snow surface temperature as estimated by Equation (3) is used to calculate out-going long-wave radiation:

$$L\uparrow = \varepsilon_s \sigma (T_s')^4 \tag{7}$$

$$L\downarrow = \varepsilon_a \sigma (T')^4 \tag{8}$$

Here, $T_s'$ and $T'$ are in Kelvin, $\sigma$ is the Stefan–Bolzmann constant, $\varepsilon_s$ (set to 0.97) is the snow surface emissivity and $\varepsilon_a$ is the emissivity from the sky, calculated according to Idso and Jackson (1969) using air temperature ($T$ in °C):

$$\varepsilon_a = 1 - 0.261 \ \exp \ (-7.77 \times 10^{-4} \ T^2) \tag{9}$$

The bulk transfer method has been found to be a simple approach suitable for the computation of turbulent fluxes ($Q_t$) in an arctic environment (Kane *et al.* 1997; Price and Dunne 1976). Appendix 1 summarizes the equations used to calculate the sensible ($Q_h$) and latent heat ($Q_e$) components.

Snowmelt computation begins at a terrain unit when its air temperature rises above 0°C. To calculate its energy fluxes, derived functions (e.g. lapse rates and wind speed modifications) are used to transfer the base station (flat site) data to the various terrain units. When $Q_m < 0$, the negative energy is considered to increase the cold content of the snowpack and all cold contents have to be overcome by subsequent positive melt energy flux before melting commences. The conversion of melt energy into melt ($M$) makes use of the latent heat of fusion ($\lambda$) and the density of water ($\rho$):

$$\begin{aligned} M &= Q_m/(\lambda\rho), \quad \text{if } Q_m > 0 \text{ and cold content is zero} \\ &= 0, \quad \text{otherwise.} \end{aligned} \tag{10}$$

#### Terrain unit snow distribution and melt

The modelling of snow distribution follows two steps: (1) hourly snowmelt at each of the 40 terrain units and (2) daily accounting of the snow water equivalent at each grid cell within the target area. The program reads in information pertaining to the base station, including its elevation, latitude and, if available, the snow temperature at the beginning of melt. It also requires the total winter snowfall recorded at the Resolute weather station. Next, the parameters for various terrain units are entered, including their mean elevations, aspects, gradients and the unit-to-base snow ratios obtained by Equation (1). Initial temperature of the snow in various terrain units is estimated based on an empirical relationship given in Equation (2). The snow temperature ($T_s$) allows the calculation of the cold content:

$$C = c\rho s'(-T_s) \tag{11}$$

where $c$ is the heat capacity of ice, $\rho$ is the density of water and $s'$ is the snow water equivalent.

Hourly meteorological data from the base station are read in, including incoming short-wave radiation, air temperature, precipitation, relative humidity, wind speed and atmospheric pressure. Incoming short-wave radiation is adjusted using Swift's (1976, Figures 1 and 2) algorithm to take account of the slope effects. Humidity is not changed but other data are extended to all the terrain units using the functions described previously and the snow surface temperatures are estimated using Equation (3). When precipitation occurs, air temperature is used to distinguish it into snowfall or rainfall, using 0°C as the criterion. With new snowfall, each terrain unit is incremented according to their unit-to-base ratios and the snow albedo is re-set to $\alpha_0$. Otherwise (i.e. no snowfall) albedo decays according to Equation (5).

The melt energy is calculated for each terrain unit and the energy balance components are summed to determine the melt energy ($Q_m$) which, if negative, is added to the cold content. Otherwise positive $Q_m$ is used to reduce the cold content and to melt the snow, with the snow storage depleted accordingly. The updated snow storage status for all terrain units ($Q_m$ converted into mm SWE and then subtracted from the residual snow in the unit) for all terrain units are sent to the output file at daily time intervals.

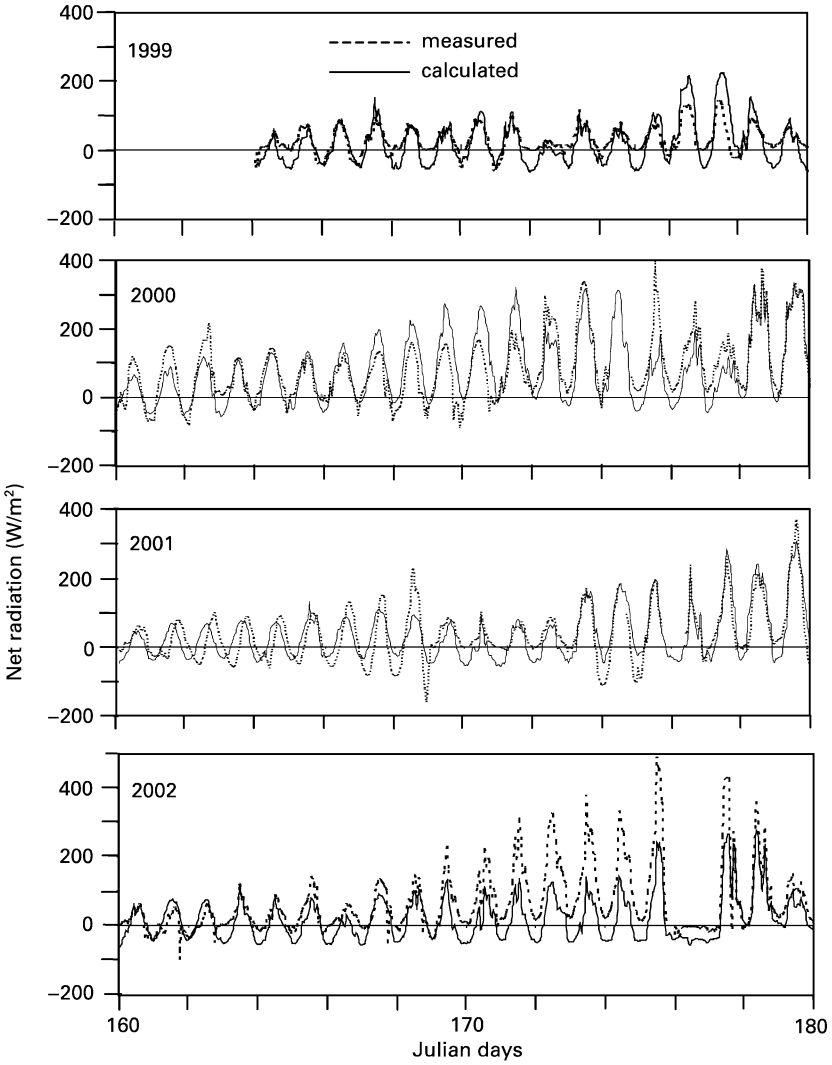


**Figure 2** Comparison of calculated and measured net radiation for the flat site during and immediately following the melt periods of 1999 to 2002

#### Snow distribution at 1 km scale

Daily snow storage values for each terrain unit are weighted against the fractional areal coverage of the units in each of the 16 × 3 grid cells to obtain the aggregate SWE for each cell. The snow storage thus calculated takes into consideration the spatial heterogeneity of snow distribution, snow accumulation and melt at the sub-grid level as it reflects the varied micro-climatic conditions at different terrain units. The daily cell snow storage values allow the distribution to be mapped for the target area at the 1 km scale.

## Results

#### Model performance

The advantage that the meso-scale models can simulate changes in snow distribution during the melt period when extensive observations are not obtainable necessarily implies that there are no available measurements to fully validate the model results. The modelled values can

be evaluated only against limited point measurements and time slices of snow cover observations.

The radiation balance (sum of net long-wave and net short-wave) computed at the site scale is compared with the measured net radiation. The simulated albedo decay follows the measured trend and the sharp albedo rise due to snowfall events is modelled correctly. The simulated pattern of net radiation variations generally follows the diurnal and seasonal measured rhythms (Figure 2). The observed and computed starting and ending dates of melt at the base station are also compared (Table 1). The correspondence of dates is within three days.

Daily depletion of the snow cover calculated for the terrain units follows a general pattern. After the air temperature at the base station becomes positive, snowmelt tends to proceed slowly for the first part of the melt season. The western rolling area has low elevation and low snow accumulation and is often the first to become bare. The dissected plateau in the north loses its snow early but the box canyons retain snow in their valleys for protracted periods. The eastern rolling area and the plateaus have similar initial snow conditions and their depletion patterns are similar. The eastern fringe has more snow and slower melt, retaining a snow cover even after most other units are snow-free. The valleys have much snow to begin with and their snow remains long after the end of the study period.

A one-time comparison of modelled fractional snow cover with satellite information is afforded by a LANDSAT-TM imagery obtained on 21 June 2000 (Figure 3). On this day, the grid cells of the eastern sector still retained a complete snow cover, which approximated the condition shown on the imagery. The snow cover in the cells dropped off abruptly in the northwest and the west, corresponding with the pattern revealed by the satellite. Although the fractional snow cover may differ for individual cells, the overall snow cover pattern across the target area was simulated realistically.

#### Aggregate properties

Large scale models usually have grid sizes with dimensions of $10-10^2$ km. The probability distribution of snow water equivalent in our $1 \times 1\,\mathrm{km}^2$ cells can describe the sub-grid variability within these large-scale grids. Figure 4 gives an example of the changes in the statistical distribution of SWE during the melt season of 1999 for the target area. The initial snow distribution on 14 June (Julian day 165) did not differ from the log-normal function (Donald *et al.* 1995; Marchand and Killingtveit 2004; Pomeroy *et al.* 1998). Melting was slow in the first two weeks but, by day 179, many parts of the western sector that consist of rolling relief underwent intense melting, giving rise to areas with low SWE. The SWE within the target area no longer followed a log-normal distribution. Melting accelerated as the snow-covered area diminished (Liston 1995) and, in early July, the snow on the eastern uplands was quickly depleted to further alter the probability distribution of SWE, giving rise to multiple modes. By 4 July (day 185), only residual snow was retained in some valleys and shaded slopes. With the emergence of many snow-free areas, the distribution gravitated towards an exponential form (or just the tail end of the truncated log-normal). If the fraction

**Table 1** Observed and simulated starting and ending dates of snowmelt at the base station

| | Beginning of melt | | End of melt | |
|---|---|---|---|---|
| Year | observed | simulated | observed | simulated |
| 1999 | 15 June | 15 June | 2 July | 29 June |
| 2000 | 10 June | 10 June | 10 June | 10 June |
| 2001 | 17 June (app) | 17 June | 26 June (app) | 26 June |

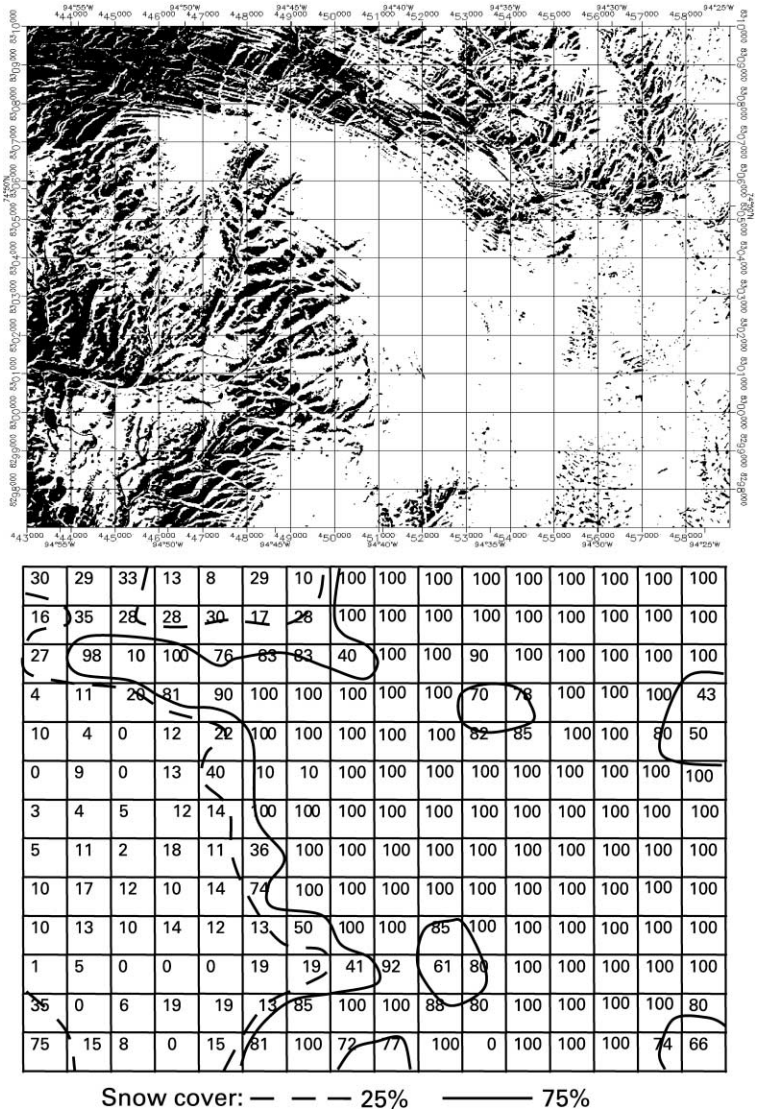


**Figure 3** Snow cover conditions in the target area on 21 June 2000: (top) LANDSAT-TM image and (bottom) simulated fractional snow cover, with numbers indicating percentage snow cover in each 1 km$^2$ grid cell

of no-snow area is included, a Weibull-like distribution can suitably describe the shape. This study indicates that uneven snowmelt in different terrain gradually transforms the log-normal distribution of SWE within an area, negating the assertion that the SWE distribution during the melt period can be depicted by a straightforward shift of the distribution curve towards decreased values and, when bare ground appears, by a simple truncation of the log-normal distribution (Donald *et al.* 1995). Such idealization may apply only to a limited area without complex terrain (cf. Luce *et al.* 1999).

The fraction of snow cover within an area is an important consideration in computing the average energy flux for large grid cells as snowmelt and evaporative losses from bare ground occur simultaneously (Liston 2004). Parameterization of the snow-covered fraction often relates the fractional snow coverage to the average snow water equivalent over an area (Luce *et al.* 1999). The mean SWE ($S$) can be calculated from the snow in each cell ($s'$):

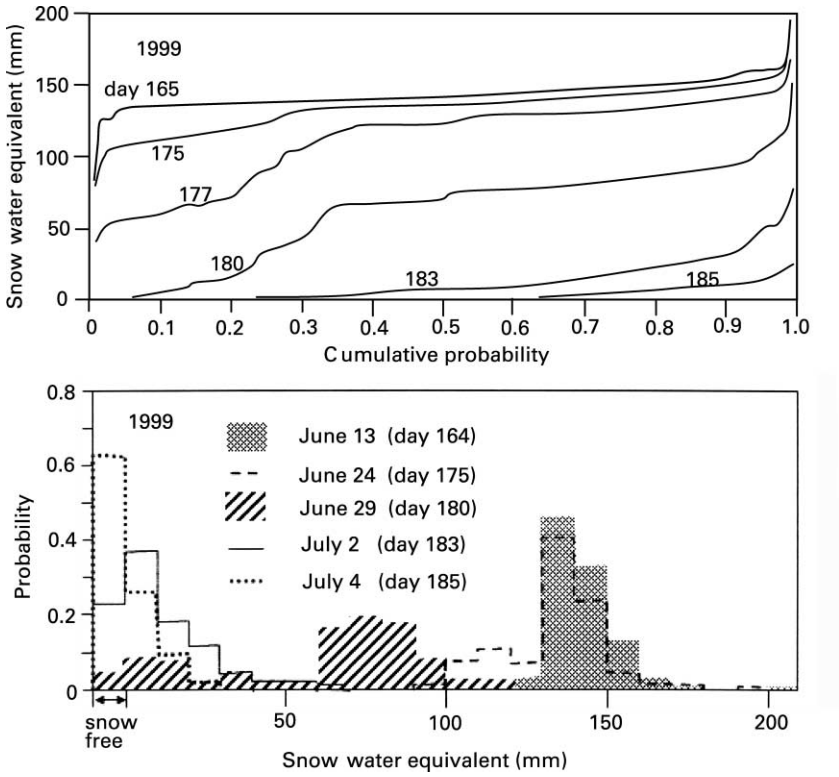


**Figure 4** Top shows cumulative probability of snow water equivalent (SWE) in the target area based on the snow in various grid cells, for different days during the melt season of 1999. Initial snow condition is indicated by the curve for 14 June (Julian day 165). Bottom shows distributions of SWE which underwent continual transformation during the melt period

$$S = \Sigma s_i'/n. \tag{12}$$

Here, $n = 208$ cells in the study area. For every day in the melt season, the ratio ($S/S_{\max}$) is calculated, with $S_{\max}$ being the maximum SWE, represented by the snow condition on the first day of melt. The daily snow-covered fraction is obtained from the model output and is plotted against $S/S_{\max}$ to produce the snow depletion curve (in the sense of Luce *et al.* (1999)).

Our depletion curve differs from that presented by Luce *et al.* (1999) who parameterize their snow depletion curve assuming uniform melt rate across their study area. In our study, different melt rates occur according to terrain. While uniform melt over an entire terrain unit is unrealistic, the approach is an improvement over the assumption of uniform melt across the whole target area. The depletion curves for four years are shown in Figure 5. They generally exhibit an S-shape, being affected by: (1) the SWE in different terrain units, (2) size of the units relative to the total area and (3) the rate of snowmelt. When large units are subject to rapid melting that depletes their thin snow cover, there is a steep drop in the curve, but if ample snow remains in spite of intense melt, the curve produces a relative flat segment. Furthermore, slow melt causes a small horizontal shift along the curve but rapid melt leads to a large horizontal shift.

The target area has three large terrain units: the plateau that occupies the centre and rolling terrain on either side of the plateau. The loss of snow from these units has

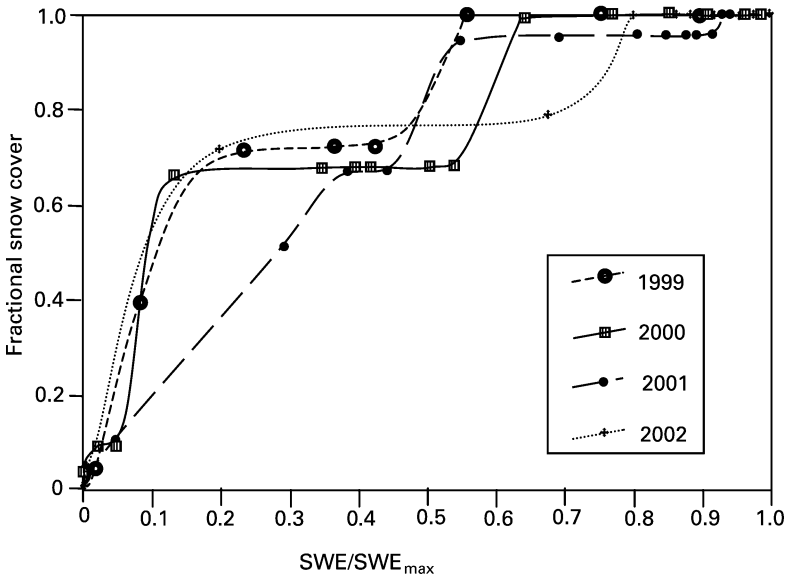


**Figure 5** Depletion curves for 1999 to 2002, showing fractional snow cover in the study area plotted against daily snow water equivalent (SWE) expressed as a ratio with the maximum or initial snow storage ($SWE_{max}$)

prominent effects on the curve. In the low snow year of 2002, the western rolling area (unit 4 in Figure 1) first lost its snow cover to cause a quick drop in the depletion curve. Subsequently, when the plateau (unit 12) and the eastern rolling terrain (unit 18) lost their snow, the depletion curve shows another plunge. In the high snow year of 2001, most of the terrain units remained snow covered until about half of the initial SWE has melted. Then, rapid melt first eliminated the snow from unit 4, and units 18 and 12 followed, causing a continuous decline in the depletion curve. A comparison of the curves for the years 1999 to 2002 indicates notable contrasts. Such between-year differences prevent the derivation of a single characteristic depletion curve to parameterize the evolution of snow ablation for a particular area.

## Conclusions

This study simulates arctic snow distribution and melt using meteorological data from a single station. It combines field investigations with modelling to simulate snow hydrology at a scale of 1 km. In the High Arctic, topography plays an important role in influencing the distribution and melting of the late-winter snow cover. Thus, terrain-driven effects on snow accumulation and melt-energy factors provide the basis for the extension of meteorological variables from a point to an area. Indexing of the snow cover using ratios of terrain unit to base station snow water equivalent is a simple approach to extend the point snow data over a large area. Field measurements of several meteorological variables made near Resolute enable the derivation of empirical relationships that relate the meteorological conditions of several terrain types to those of the base station located at a coastal, lowland site.

The snow cover indexing method and the field-derived transfer functions are employed in a model to extend the meteorological input data obtained from a point to various terrain units found in the study area. The end-of-winter snow distribution over a $16 \times 13\,km^2$ target area is first simulated. Snow melt at individual terrain units is computed using the energy balance approach and the melt rates are weighted by the fraction of areal coverage of the various terrain units within each $1 \times 1\,km^2$ grid cell. The data allow the changing snow pattern to be mapped at daily intervals during the melt seasons.

Meso-scale models such as the one described offers simulated snow data for an area. At this intermediate (1 km) scale, the entire targeted simulation area would be encompassed by a single grid cell in most land surface schemes or regional models. The simulated results are useful for studying sub-grid variability and permit the testing of assumptions made in large-scale modelling. One assumption is that the snow distribution follows an unchanging, though continuously truncated, log-normal distribution during the melt season. This assertion is predicated upon uniform melt rate across the grid area which cannot hold for heterogeneous terrain or over large areas. Our results demonstrate a continuous transformation of the statistical distribution during melt, stretching the log-normal distribution and creating multiple modes until towards the end of snowmelt when the abundance of bare ground and low residual snow conditions lead to an exponential-type distribution. Thus, the present study does not support the universality that the log-normal SWE distribution is preserved during the melt season.

The simulated snow conditions also permit the construction of snow depletion curves which relate fractional snow cover to the snow water equivalent in an area, a device that is used by macro-scale models to parameterize sub-grid variability of snow. There is considerable year-to-year variations in the curve, depending on the initial amount (not the spatial distribution pattern) of snow and on the differential melt rates over the target area, rendering it difficult to obtain a single curve to characterize the trajectory of snow loss in a particular area. This unfortunately complicates the parameterization of snow depletion for large-scale modelling.

## Acknowledgements

This work is funded by research grants from the Natural Sciences and Engineering Research Council of Canada, and by research contracts from the Meteorological Service of Canada through Dr Barry Goodison. Generous logistical support in the field was given by the Polar Continental Shelf Project, Natural Resources Canada. The reviewers provided critical comments on this paper, for which we are grateful.

## References

Brutsaert, W. (1975). On a derivable formula for long-wave radiation from clear skies. *Water Res. Res.*, **11**, 742–744.

Déry, S.J. and Yau, M.K. (2001). Simulation of blowing snow in the Canadian Arctic using a double-moment model. *Boundary-Layer Meteorol.*, **99**, 287–316.

Donald, J.R., Soulis, E.D. and Kouwen, N. (1995). A land cover-based snow cover representation for distributed hydrologic models. *Water Res. Res.*, **31**, 995–1009.

Essery, R.L.H., Li, L. and Pomeroy, J.W. (1999). A distributed model of blowing snow over complex terrain. *Hydrol. Process*, **13**, 2423–2438.

Frei, A. and Robinson, D.A. (1998). Evaluation of snow extent and its variabilty in the Atmospheric Model Intercomparison Project. *J. Geophys. Res.*, **103**(D8), 8859–8871.

Goodison, B.E. (1978). Accuracy of Canadian snow gage measurements. *J. Appl. Meteorol.*, **27**, 1542–1548.

Idso, S.B. and Jackson, R.D. (1969). Thermal radiation from the atmosphere. *J. Geophys. Res.*, **74**(23), 5397–5403.

Kane, D.L., Gieck, R.E. and Hinzman, L.D. (1997). Snowmelt modeling at a small Alaskan Arctic watershed. *J. Hydrol. Eng.*, **2**, 204–210.

Liston, G.E. (1995). Local advection of momentum, heat and moisture during the melt of patchy snow covers. *J. Appl. Meteorol.*, **34**, 1705–1715.

Liston, G.E. (2004). Representing subgrid snow cover heterogeneities in regional and global models. *J. Climate*, **17**, 1381–1397.

Liston, G.E. and Sturm, M. (1998). A snow-transport model for complex terrain. *J. Glaciol.*, **44**, 498–516.

Luce, C.H., Tarboton, D.G. and Cooley, K.R. (1999). Sub-grid parameterization of snow distribution for an energy and mass balance snow cover model. *Hydrol. Process*, **13**, 1921–1933.

Marchand, W.-D. and Killingtveit, Å. (2004). Statistical properties of spatial snowcover in mountainous catchments in Norway. *Nordic Hydrol.*, **35**, 101–108.

Pomeroy, J.W. and Essery, R. (1999). Turbulent fluxes during blowing snow: field tests of model sublimation predictions. *Hydrol. Process*, **13**, 2963–2975.

Pomeroy, J.W., Shook, K.R., Toth, B., Essery, R.L.H., Pietroniro, A. and Hedstrom, N. (1998). An evaluation of snow accumulation and ablation processes for land surface modeling. *Hydrol. Process*, **12**, 2339–2367.

Price, A.J. and Dunne, T. (1976). Energy balance computations of snowmelt in a subarctic area. *Water Res. Res.*, **12**, 686–694.

Shiklomanov, A.I., Lammers, R.B. and Vörösmarty, C.J. (2002). Widespread decline in hydrological monitoring threatens pan-Arctic research. *EOS*, **83**(2), 13–17.

Swift, L.W. (1976). Algorithm for solar radiation on mountain slopes. *Water Res. Res.*, **12**, 108–112.

Woo, M.K. (1998). Arctic snow cover information for hydrological investigations at various scales. *Nordic Hydrol.*, **29**, 245–266.

Woo, M.K. and Dubreuil, M.-A. (1985). Empirical relationship between dust content and Arctic snow albedo. *Cold Regions Sci. Technol.*, **10**, 125–132.

Woo, M.K. and Ohmura, A. (1997). The Arctic Islands. In: *The Surface Climates of Canada*, W.G. Bailey, T. Oke and W.R. Rouse (Eds), Montreal, McGill-Queen's University Press, pp. 172–197.

Woo, M.K., Walker, A., Yang, D. and Goodison, B. (1995). Pixel-scale ground snow survey for passive microwave study of the arctic snow cover. In: *Proceedings 52nd Eastern Snow Conference, Toronto*, M.R. Albert and S. Taylor (Eds), pp. 51–57.

Woo, M.K., Yang, D. and Young, K.L. (1999). Representativeness of arctic weather station data for the computation of snowmelt in a small area. *Hydrol. Process*, **13**, 1859–1870.

Yang, D. and Woo, M.K. (1999). Subgrid variability of maximum snow cover in the Canadian High Arctic. *Hydrol. Process*, **13**, 1977–1988.



## Appendix 1

The bulk transfer equations used to compute the sensible ($Q_h$) and latent heat ($Q_e$) fluxes are

$$Q_h = \rho_a \ C_a \ Du_z \ (T_z - T_s) \tag{A1}$$

$$Q_e = \rho_a \ \lambda_v \ (\mu/P) \ Du_z \ (e_z - e_s) \tag{A2}$$

where $T_z$ and $T_s$ are temperatures at height $z$ and at the snow surface; $e_z$ and $e_s$ are the vapour pressure at height $z$ and at the snow surface, the latter being taken to be the saturation vapour pressure at $T_s$; $\rho_a$ is air density; $C_a$ is heat capacity of air; $\lambda_v$ is latent heat of vaporization; $\mu$ is the ratio of molecular weights of water and air; $P$ is atmospheric pressure; $u_z$ is wind speed at height $z$; $D$ is a drag coefficient, assumed to be the same for both fluxes:

$$D = \kappa^2/[\ln(z/z_0)]^2 \tag{A3}$$

with $\kappa$ being the von Kármán constant, $z$ the height of the instrument and $z_0$ the surface roughness.

The drag coefficient is adjusted for stability conditions based on the Richardson number ($R$):

$$\begin{aligned} D_s &= D/(1 + \sigma R) \\ D_u &= D(1 - \sigma R) \end{aligned} \tag{A4}$$

where the subscripts $s$ and $u$ denote stable and unstable conditions, and $\sigma$ is a coefficient with the value of 10.